Journal of Materials Chemistry A

ROYAL SOCIETY OF CHEMISTRY

PAPER

View Article Online
View Journal | View Issue

Cite this: J. Mater. Chem. A, 2022, 10, 25356

CO_2-to-CH_4 electroreduction over scalable Cu-porphyrin based organic polymers promoted by direct auxiliary bonding interaction†

Qi Li, [a] Zeng-Mei Wang, *[a] Yifa Chen, *[b] Yi-Rong Wang,[c] Can Guo,[b] Qing Huang,[b] Long-Zhang Dong, [c] Shun-Li Li[b] and Ya-Qian Lan *[b]

The scale-up syntheses of electrocatalysts with rationally designed functional promoter groups that can directly interact with catalytic-centres are much desired for CO_2 electroreduction. Here, we propose an *in situ* copolymerization method that can be applied for the scale-up syntheses of metalloporphyrin based conjugated porous polymers with directly interacting catalytic centres and promoter groups. The thus-obtained materials possess the characteristics of high porosity, adjustable morphology, abundant catalytic sites and directly interacting promoter groups. In particular, CPP–Cu with ferrocene as the promoter group exhibits a $FE_{CH_4+C_2H_4}$ of 94.0% (FE_{CH_4}, 75.9%, $FE_{C_2H_4}$, 18.1%, −0.9 V), which is much higher than that of Cu-porphyrin, Bz-CPP-Cu and the physical-mixture and represents one of the best electro-catalysts so far. DFT calculations reveal that the directly-interacting ferrocene groups could enhance the electron-cloud density of Cu-porphyrin and possess strong adsorption-ability to OH* to kinetically improve the proton-coupled electron transfer for the preferential CO_2-to-CH_4 pathway. Noteworthily, the synthesis-strategy is easy to scale-up (~10 g in a batch-experiment) and the reaction-time can be as little as 10 min under microwave-conditions.

Received 27th July 2022
Accepted 5th November 2022

DOI: 10.1039/d2ta05934g

rsc.li/materials-a

Introduction

The electrochemical CO_2 reduction reaction (CO_2RR) is a significant strategy for sustainable energy conversion and alleviating climate change since it allows for CO_2 conversion into valuable chemicals/fuels using renewable electricity.[1,2] In particular, the highly selective production of higher value-added fuels (*e.g.*, CH_4, C_2H_4, C_2H_5OH, *etc.*) has received tremendous attention due to their dominant positions in energy supply for both human life and industrial production.[3] Nevertheless, their production processes generally require sufficient and highly active redox centres to realize the challenging proton-coupled electron transfer (PCET) steps including intermediate generation, conversion or utilization.[4,5] Generally, it is difficult for electrocatalysts with single-functional sites to produce such advanced products with high efficiency, thus some functional auxiliary groups (*e.g.*, electron donating groups,[6] CO generation sites,[7] intermediate stabilizers[8] or electron conducting groups,[9] *etc.*) are of vital importance to assist the improvement of CO_2RR performances. Even so, the rational and controllable design of functional auxiliary groups with suitable interaction distance to catalytic sites, controllable morphology and clear interaction mechanisms are still rare. Besides, the investigation of scale-up strategies for CO_2RR electrocatalysts especially that can efficiently generate higher-value added products is much needed. Thus, it would be quite interesting to explore facile strategies that enable the scale-up syntheses of electrocatalysts with directly interacting and adjustable auxiliary groups for efficient generation of higher-value products.

Metalloporphyrins or their derivatives are promising candidates for the electrocatalytic CO_2RR owing to their planar and conjugated structure, high activity and easy accessibility.[10] Among them, Cu-porphyrin with $Cu–N_4$ sites has been widely investigated as a potential electrocatalyst for higher value-added products,[11,12] yet is still restricted by the stacking effect, low stability or lack of functionality, *etc.* Generally, strategies focused on embedding the Cu-porphyrin units in porous structures like metal–organic frameworks (MOFs), covalent-organic frameworks (COFs) or porous organic polymers (POPs) to prevent the unit from stacking, improve the stability and facilitate the mass transfer efficiency.[1,13] To enrich the properties of the Cu-porphyrin unit, various auxiliary groups have been introduced and studied in Cu-porphyrin-based porous materials, and the strategies can be mainly concluded as the

[a]Jiangsu Key Laboratory of Construction Materials, College of Materials Science and Engineering, Southeast University, No. 2, Southeast University Road, Nanjing 211189, P. R. China. E-mail: 101011338@seu.edu.cn

[b]School of Chemistry, South China Normal University, Guangzhou, 510006, P. R. China. E-mail: chyf927821@163.com; yqlan@njnu.edu.cn

[c]School of Chemistry and Materials Science, Nanjing Normal University, Nanjing 210023, P. R. China

† Electronic supplementary information (ESI) available: Experimental methods and supporting figures and tables. See DOI: https://doi.org/10.1039/d2ta05934g

following three: (1) direct growth of powerful units like polyoxometalates (POMs), thiophene and cucurbituril in the porous structures through coordination or covalent connections;[14–18] (2) post-modification of porous frameworks with functional groups like pyrrolidine azide or rhenium bipyridine[19–21] and (3) incorporation of powerful auxiliary groups such as ferrocene or polypyrrole in the pores.[22–24] In general, there exists a cut-off radius for the auxiliary unit to the functional centre that is set to be only several angstroms based on the concept of nearsightedness, and minor effect of the CO_2RR auxiliary with longer distance to the functional units would be achieved in theoretical calculations, which is commonly applied in reproducing the calculation results of large systems using high dimensional neural network potentials (HDNNPs).[25–27] However, most of the reported Cu-porphyrin based porous electrocatalysts obtained through these strategies are still limited by the unreached cut-off distance of the auxiliary unit to the active Cu-porphyrin centres, resulting in the indirect interaction and unmet performances. The molecular-level design of task-specific and directly-interacting CO_2RR auxiliary units to match with the need for corresponding proton-coupled electron-transfer steps is still a challenging task. Besides, the general synthesis strategies for Cu-porphyrin based porous electrocatalysts are still difficult for scale up production, which are mostly time and energy consuming.[28,29] In this regard, it is essential to explore facile and scalable strategies that enable molecular-level design of Cu-porphyrin based CO_2RR electrocatalysts with directly interacting auxiliary units on the catalytic centres for the production of higher-value products.

Here, we report a facile and scalable strategy to prepare a series of Cu-porphyrin based conjugated porous polymers (*e.g.*, Fc-CPP-Cu, Bz-CPP-Cu, Bp-CPP-Cu and Tp-CPP-Cu) by *in situ* copolymerization of dialdehyde-based ligands and pyrrole, and successfully apply them in efficient electrocatalytic CO_2-to-CH_4 conversion (Scheme 1). The thus-obtained materials possessing high porosity, adjustable morphology and high stability are composed of directly bonded auxiliary groups and Cu-porphyrin centres, which would be much beneficial for the enhancement of CO_2RR performance. Specifically, Fc-CPP-Cu with ferrocene as the promoter group exhibits a $FE_{CH_4+C_2H_4}$ of 94.0% (FE_{CH_4}, 75.9% and $FE_{C_2H_4}$, 18.1%, −0.9 V), which is much higher than that of Cu-porphyrin, Bz-CPP-Cu and the physical mixture and represents one of the best CO_2 electroreduction catalysts so far. DFT calculations reveal that the directly interacting ferrocene groups enhance the electron-cloud density of Cu in the porphyrin-centre. Meanwhile, the strong adsorption ability of ferrocene groups to OH* promotes the proton-coupled electron transfer (PCET) reaction process, which kinetically improves the preferential CO_2-to-CH_4 pathway. This strategy based on the direct-bonding method provides a promising reference for the design of powerful metalloporphyrin based electrocatalysts.

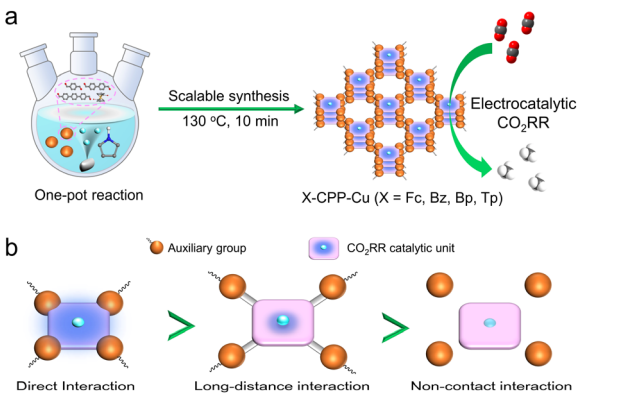

Scheme 1 The schematic illustration of X-CPP-Cu (X = Fc, Bz, Bp and Tp) in the electrocatalytic CO_2RR. (a) The scalable synthesis of X-CPP-Cu (X = Fc, Bz, Bp and Tp). (b) The advantage of direct bonding interaction in the electrocatalytic CO_2RR.

Results and discussion

Characterization of the materials

The syntheses of porphyrin based conjugated porous polymers (*e.g.*, Fc-CPP-Cu, Bz-CPP-Cu, Bp-CPP-Cu and Tp-CPP-Cu) were carried out by the *in situ* copolymerization of dialdehyde-based ligands and pyrrole in propionic acid solution (Fc, Bz, Bp and Tp stand for ferrocenyl, benzene, biphenyl and triphenyl, respectively) (for details see the Methods) (Scheme 1). For example, the synthetic process of Fc-CPP-Cu includes the copolymerization of 1,1′-ferrocenedicarboxaldehyde and pyrrole in the presence of $Cu(CH_3COO)_2 \cdot H_2O$ and propionic acid, during which propionic acid catalyzes the reaction and Cu^{2+} simultaneously coordinates to the porphyrin-center in the *in situ* generated Fc-CPP-Cu.

To characterize it, various tests have been conducted and analyzed. Powder X-ray diffraction (PXRD) patterns of these samples show a broad diffraction peak in the 2θ range from 10 to 35°, indicating their amorphous nature (Fig. S1†). To demonstrate the chemical composition, we further performed Fourier transform infrared (FTIR) spectroscopy and X-ray photoelectron spectroscopy (XPS) analyses (Fig. 1a and S2†). Taking Fc-CPP-Cu as an example, the peaks at 1490, 1186 and 516 cm^{-1} can be seen as the infrared absorption peaks of ferrocene, indicating the existence of ferrocene in Fc-CPP-Cu.[30] Furthermore, the C=O bond (1651 cm^{-1}) disappears when compared to ferrocene dialdehyde in the FTIR spectrum, suggesting the successful conversion of the aldehyde group (Fig. 1a).[31] In addition, the absorption peak of Cu–N (~1000 cm^{-1}) agrees well with the peak position of tetraphenylporphyrin-Cu (TPP-Cu), indicating that the metal coordination occurs at the porphyrin center.[32] In the XPS test, the N 1s spectrum (Fig. S2a†) presents two major peaks at 399.3 and 400.6 eV, which are assigned to Cu–N_4 and pyrrolic-N, respectively.[33,34] The XPS spectrum of Fc-CPP-Cu shows two peaks (721.3 eV, $2p_{1/2}$ and 707.8 eV, $2p_{3/2}$) that can be attributed to the Fe 2p spin–orbit splitting (Fig. S2b†).[30,34,35] This indicates that Fe(II) in Fc-CPP-Cu remains in the low-spin +2 oxidation state, consistent with that of ferrocene. As shown in Fig. S3,† Bz-CPP-Cu, Bp-CPP-Cu and Tp-CPP-Cu show similar absorption peaks of N–Cu in FTIR spectra at ~1000 cm^{-1}, suggesting the existence of Cu-porphyrin in these samples. Furthermore, no

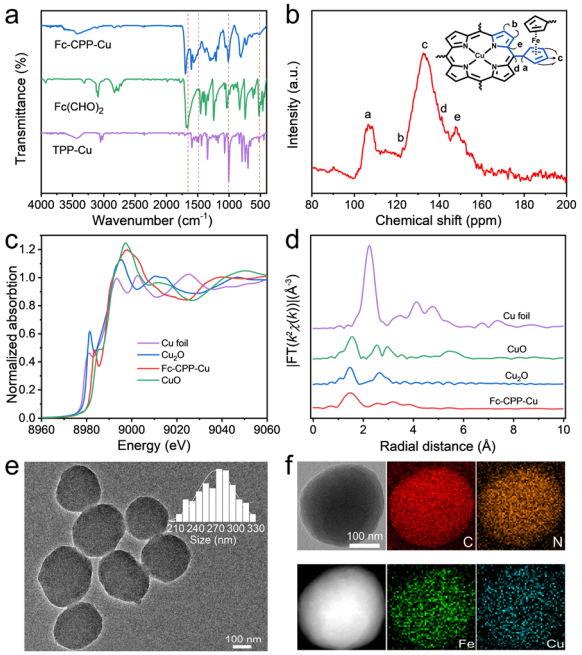

Fig. 1 The characterization of Fc-CPP-Cu. (a) The FTIR spectra. (b) Solid-state ^{13}C CP/MAS spectrum of Fc-CPP-Cu. (c) Cu K-edge XANES spectra of Cu foil, Cu_2O, CuO, and Fc-CPP-Cu. (d) Cu K-edge FT spectra of Cu foil, Cu_2O, CuO, and Fc-CPP-Cu. (e) TEM image of Fc-CPP-Cu. (f) STEM and mapping images of Fc-CPP-Cu.

characteristic peak of pyrrole has been detected in these samples, proving no residual pyrrole in these samples. In addition, the solid-state ^{13}C NMR spectrum (Fig. 1b) of Fc-CPP-Cu exhibits five peaks (a–e), which are attributed to the five-membered rings on ferrocene (peaks a and c) and porphyrin (peaks b, d and e) units, respectively.[31,36,37] To further investigate the structure of Fc-CPP-Cu, X-ray absorption near edge structure (XANES) and extended X-ray absorption fine structure (EXAFS) spectroscopy have been conducted to confirm the structure of Fc-CPP-Cu. According to the normalized XANES spectra of Fc-CPP-Cu and several reference materials including CuO, Cu_2O and Cu foil, the absorption edge position of Fc-CPP-Cu is located similar to that of CuO, indicating that the Cu species in Fc-CPP-Cu is present as Cu(II) (Fig. 1c). Besides, no obvious signal of the Cu–Cu bond is observed in the EXAFS (Fig. 1d).[38–40] Similarly, XANES and EXAFS spectra of Fc-CPP-Cu also support the existence of Fe(II) in ferrocene groups (Fig. S4†).[41] All this evidence suggest that dialdehyde-based ligands and pyrrole are successfully polymerized in these samples.

To evaluate the porosity of these samples, N_2 sorption tests at 77 K have been carried out to determine the porosity and specific surface area. The adsorption–desorption curves of Fc-CPP-Cu exhibit typical type II isotherms, revealing the presence of micropores in Fc-CPP-Cu (Fig. S5a†). The Brunauer–Emmett–Teller surface area (S_{BET}) of Fc-CPP-Cu is calculated to be 144 $m^2\ g^{-1}$ with a total pore volume (V_t) of 0.18 $cm^3\ g^{-1}$. In addition, quenched solid-state density functional theory (QSDFT) calculation reveals that Fc-CPP-Cu possesses a relatively narrow pore size distribution centered at ~1.28 nm (Fig. S5b†). In addition, the S_{BET} of Bz-CPP-Cu, Bp-CPP-Cu and Tp-CPP-Cu was calculated to be 60.73 $m^2\ g^{-1}$, 17.00 $m^2\ g^{-1}$ and 14.03 $m^2\ g^{-1}$, respectively (Fig. S6†). To evaluate the CO_2 absorption capacity of Fc-CPP-Cu, CO_2 absorption tests were performed and Fc-CPP-Cu presented CO_2 uptake capacities of 61.5 $cm^3\ g^{-1}$ and 34.2 $cm^3\ g^{-1}$ at 273 K and 298 K, respectively. As a comparison, the CO_2 absorption capacities of Bz-CPP-Cu (30.5 $cm^3\ g^{-1}$, 273 K and 17.5 $cm^3\ g^{-1}$, 298 K), Bp-CPP-Cu (16.2 $cm^3\ g^{-1}$, 273 K and 11.0 $cm^3\ g^{-1}$, 298 K) and Tp-CPP-Cu (10.9 $cm^3\ g^{-1}$, 273 K and 7.4 $cm^3\ g^{-1}$, 298 K) are all lower than that of Fc-CPP-Cu, implying the superior effect of ferrocene on CO_2 adsorption (Fig. S7†).

As detected in the transmission electron microscopy (TEM) test, Fc-CPP-Cu displays round nanosphere morphology with an average diameter of ~275 nm (Fig. 1e). Elemental mapping images (Fig. 1f) show that the elements of C, N, Fe and Cu are uniformly dispersed in the nanospheres, implying the homogeneously distributed nature of both Cu-porphyrin and ferrocene groups. In addition, energy dispersive spectroscopy (EDS) elemental analysis of Fc-CPP-Cu presents ~12.8 and ~9.2 wt% weight percentage for Fe and Cu (Fig. S8†), respectively, which agrees well with the results of inductively coupled plasma optical emission spectrometry (~13.1 and 9.4 wt%) (Table S1†). Moreover, the high-resolution TEM (HRTEM) image shows that the microspheres have an amorphous structure (Fig. S9†), which is consistent with the PXRD results. Bz-CPP-Cu, Bp-CPP-Cu and Tp-CPP-Cu also exhibit similar nanosphere morphology as supported by the SEM tests (Fig. S10†). Thus, we have obtained a series of Cu-porphyrin based conjugated porous polymers with adjustable morphology, abundant catalytic sites and directly interacting promoter groups, which might serve as promising candidates for the electrocatalytic CO_2RR.

Electrochemical carbon dioxide reduction performance

In order to evaluate the electrocatalytic CO_2RR performance, electrochemical tests were performed in a flow cell at different potentials. Gas diffusion layer (GDL) modified carbon paper coated with the catalyst was used as the working electrode. In all experiments, a peristaltic pump was used to flow 1 M KOH electrolyte at 7 mL min^{-1} into the anode and cathode chambers, and a mass flow controller was used to pass CO_2 through the GDL at a flow rate of 20 sccm. The substantially large current density was achieved because the mass transfer of CO_2 along the triple-phase boundary was greatly enhanced in the GDL.[42–45] The basic model of the flow cell test setup is shown in Fig. S11.† In this work, all potentials were measured with the Ag/AgCl electrode and the results are reported relative to the reversible hydrogen electrode (RHE).

For a preliminary performance evaluation, linear sweep voltammetry (LSV) curves were first measured to assess the electrocatalytic activity at applied potentials from 0 to −1.1 V *vs.* RHE. As shown by the LSV polarization curves, Fc-CPP-Cu shows a total current density of −491.5 mA cm^{-2} at −1.1 V, which is much better than that of Bz-CPP-Cu (−344.9 mA cm^{-2}), Bp-CPP-Cu (−244.8 mA cm^{-2}) and Tp-CPP-Cu (207.3 mA cm^{-2}), indicating its higher electrocatalytic activity (Fig. 2a and S12†).

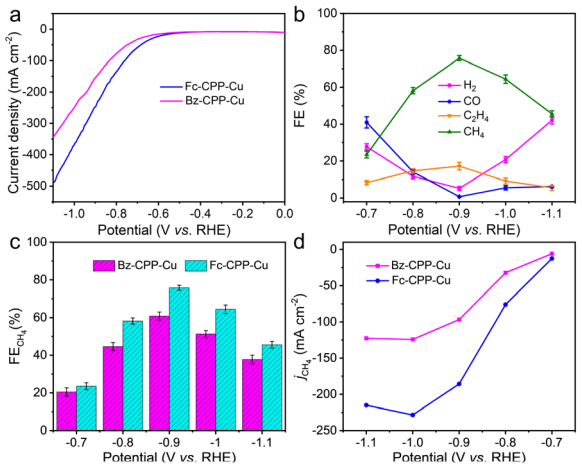

Fig. 2 Electrocatalytic performance of Fc-CPP-Cu and Bz-CPP-Cu. (a) LSV curves. (b) Faradaic efficiencies of CO_2RR products at different applied potentials for Fc-CPP-Cu. (c) FE for CH_4 at different applied potentials. (d) Partial CH_4 current density.

By comparing with the LSV results tested under an Ar atmosphere, Fc-CPP-Cu shows lower onset potential and higher current density under a CO_2 atmosphere, indicating that the high electrochemical performance of Fc-CPP-Cu originates from the CO_2RR (Fig. S13a†). To further evaluate the selectivity of the catalysts, electrolysis experiments were performed at selected potentials from −0.7 to −1.1 V *vs.* RHE. The results show that the electrocatalytic CO_2 reduction products are CH_4, C_2H_4, CO, and H_2 (Fig. 2b). Besides, the faradaic efficiency (FE) values of the products were calculated for different applied potentials and the total FE of all potentials was ~100%. Fc-CPP-Cu gives the highest FE_{CO} (38.2%) as well as 26.4% FE_{H_2}, 21.7% FE_{CH_4} and negligible $FE_{C_2H_4}$ at −0.7 V with a current density of −56.2 mA cm^{-2} (Fig. 2b and S13a†). After that, the FE_{CO} continues to decrease with the increase of potential. FE_{CH_4} continuously increases in the applied potential range from −0.7 to −0.9 V, reaching a maximum value of ~75% at −0.9 V and remaining above 60% in the potential range from −0.8 to −1.0 V in 1 M KOH solution (Fig. 2b). Specifically, Fc-CPP-Cu exhibits a large active current density and high CH_4 selectivity at a low reductive potential, outperforming most of the reported Cu-based CO_2RR systems in both flow cell and H-type cell systems (Table S2†). Noteworthily, the total $FE_{CH_4+C_2H_4}$ of Fc-CPP-Cu is up to 94.0% at −0.9 V and remains above 70% in the potential range from −0.7 to −1.0 V (Fig. S14†).

In addition, Bz-CPP-Cu, Bp-CPP-Cu and Tp-CPP-Cu with different aldehyde groups were also tested by CO_2RR experiments. The results show that Bz-CPP-Cu, Bp-CPP-Cu and Tp-CPP-Cu can reach up to the highest FE_{CH_4} of 62.7% (−0.9 V), 45.8% (−1.0 V) and 44.3% (−1.0 V), respectively, implying that Fc-CPP-Cu is the best one among them in the electrocatalytic CO_2RR (Fig. S15–S17†). Besides, TPP-Cu and the physical-mixture of ferrocene and TPP-Cu (molar ratio, ferrocene/TPP-Cu = 2 : 1) have been tested as the contrast samples. The results show that TPP-Cu and the physical-mixture display FE_{CH_4} values of only 27.5% (−1.1 V) and 37.4% (−0.9 V), which are much lower than that of Fc-CPP-Cu (Fig. S18†). To further support the superior performance of Fc-CPP-Cu, Fc-CPP (porphyrin center without Cu) and ferrocene were also tested and presented no CO_2RR activity (Fig. S18†). Based on the above-mentioned results, the superior performance of Fc-CPP-Cu would be attributed to the synergistic effect of ferrocene groups and Cu-porphyrin centers in the electrochemical CO_2RR.

To further investigate the activity of Fc-CPP-Cu, partial current densities were calculated for CH_4, CO, C_2H_4 and H_2 at different potentials (Fig. 2d and S13b†). Due to the similarity of Bz-CPP-Cu, Bp-CPP-Cu and Tp-CPP-Cu, we selected Bz-CPP-Cu as the contrast sample to be compared with Fc-CPP-Cu. Notably, Fc-CPP-Cu shows a CH_4 partial current density of −185.8 mA cm^{-2} at −0.90 V, which is almost 2 times higher than that of Bz-CPP-Cu (−96.7 mA cm^{-2}) (Fig. 2d). In addition, the turnover frequency (TOF, s^{-1}) of Fc-CPP-Cu has been tested and the TOF was calculated to be 0.013 s^{-1} at −0.9 V. To reveal the carbon source of CO_2RR products, isotope experiments were performed under the same reaction conditions with $^{13}CO_2$ as the substrate. The products were analyzed by gas chromatography and mass spectroscopy. As shown in Fig. 3a and S19,† $^{13}CH_4$, ^{13}CO and $^{13}C_2H_4$ are detected with corresponding peaks at m/z = 17, 29 and 30, respectively, indicating that the carbon sources of CH_4, CO and C_2H_4 indeed derive from the CO_2 conversion.

In addition, the superior CO_2RR performance of Fc-CPP-Cu suggests that it may possess high electrochemically active surface area (ECSA). To investigate the deeper influences on the significant performance of Fc-CPP-Cu, the electrochemical double-layer capacitance (C_{dl}) was calculated to evaluate the ECSA (Fig. S20†). The results show that the C_{dl} value (14.61 mF cm^{-2}) of Fc-CPP-Cu is larger than that of Bz-CPP-Cu (11.41 mF cm^{-2}). This indicates that Fc-CPP-Cu possesses a larger available catalytic area and more effective electrocatalytic active sites in contact with the electrolyte, thus improving the CO_2RR

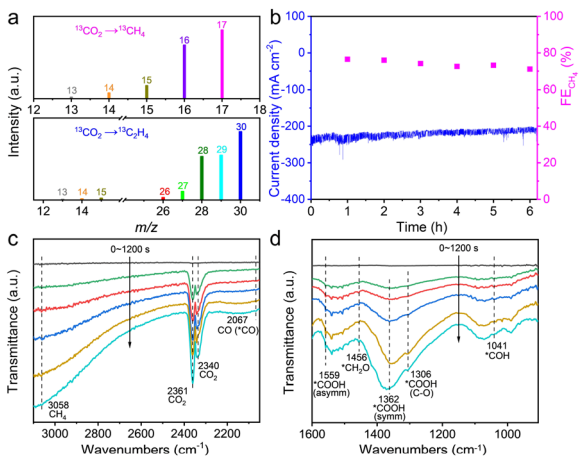

Fig. 3 CO_2RR performance of Fc-CPP-Cu. (a) The mass spectra of $^{13}CH_4$ and $^{13}C_2H_4$ recorded under a $^{13}CO_2$ atmosphere. (b) Durability test of Fc-CPP-Cu at a potential of −0.9 V *vs.* RHE. (c and d) *In situ* ATR-FTIR spectra of Fc-CPP-Cu during the electrochemical CO_2RR.

performance. Furthermore, to investigate the electrocatalytic kinetics of Fc-CPP-Cu and Bz-CPP-Cu at the electrode/electrolyte surface during the electrochemical CO_2RR, electrochemical impedance spectroscopy (EIS) spectra of the samples were recorded at a potential of −0.9 V *vs.* RHE (Fig. S21†). As shown in the Nyquist plots, Fc-CPP-Cu exhibits smaller charge transfer resistance (12.17 Ω) than that of Bz-CPP-Cu (20.08 Ω), which implied that Fc-CPP-Cu is able to provide faster electron transfer from the catalyst surface to the reactants in the intermediate generation, ultimately leading to an increase in activity and selectivity.

Stability is a vital factor to evaluate the durability of catalysts in the electrocatalytic CO_2RR. To investigate the electrochemical stability of Fc-CPP-Cu, the chronoamperometry curve was applied to evaluate the durability over a long time at −0.9 V (Fig. 3b). After 6 h, the FE_{CH_4} of Fc-CPP-Cu can be maintained above 70% and the current density remained at approximately −200 mA cm^{-2}. For the leaching test, ICP-MS results showed that the Cu detected in the solution phase was below the detection limit (Table S3†). In addition, the chemical state of Cu species after electrocatalysis was also evaluated by the XPS test (Fig. S22†). After the test, the Cu 2p spectra of the Fc-CPP-Cu electrodes are similar to those before the test, and no Cu or Cu(I) is observed. In addition, XANES and EXAFS tests have also been performed to support the stability. The results show that no significant change in Cu K-edges and no visible metallic Cu signals are observed in the XANES profiles of Fc-CPP-Cu before and after the CO_2RR process (Fig. S23a†). Besides, no obvious signal of the Cu–Cu bond is observed in the EXAFS spectrum (Fig. S23b†).[38–40] Similarly, the ferrocene functional group in Fc-CPP-Cu also did not change before and after the CO_2RR processes as supported by the unchanged Fe(II) signals in the XANES and EXAFS spectra of Fc-CPP-Cu (Fig. S24†).[41]

Thus, we have obtained a kind of stable electrocatalyst with efficient electrocatalytic CO_2RR performance through a facile method. Based on the above-mentioned interesting results, we further extend the facile method to investigate both scale-up and fast syntheses. Firstly, we have conducted the scale-up synthesis under identical conditions and increased the amount of the reactants to 20 times higher than the original one. ∼10 g Fc-CPP-Cu could be obtained in a batch experiment as supported by the SEM and FTIR tests (Fig. S25–S27†). Interestingly, it shows the retention of round nanosphere morphology yet the diameter is increased from ∼275 nm to ∼1 μm. Electrocatalytic CO_2RR tests show that it has slightly decreased performance (FE_{CH_4}, 63%; $FE_{CH_4+C_2H_4}$, 77%, −0.9 V), which might be attributed to the enhanced particle size (Fig. S28†). Secondly, Fc-CPP-Cu can be readily produced under applied microwave-assisted heating conditions and the reaction time can be as less as 10 min (Fig. S27 and S29†). After the reaction, it possesses relatively irregular nanoparticle morphology and slightly decreased performance (FE_{CH_4}, 59%; $FE_{CH_4+C_2H_4}$, 66%, −0.9 V) (Fig. S30†). Therefore, the facile method enables fast and scale-up production of electrocatalysts that can efficiently generate higher-value products, which will be much beneficial for industrial-level electrocatalytic CO_2RR applications.

Investigation of the catalytic mechanism

In addition, DFT calculations were performed to understand the reason for the superior performance of Fc-CPP-Cu. As shown in Fig. 4c, the *COOH adsorption energy is smaller than that of *H for both Fc-CPP-Cu and Bz-CPP-Cu (Fig. S31†), thus ensuring a higher selectivity for CH_4. This is also consistent with the higher FE_{CH_4} than for the HER detected in the experimental results. We also noticed that the rate determining step was CO_2 → *COOH for both Fc-CPP-Cu and Bz-CPP-Cu in the CO_2RR pathway (Fig. S31†). Besides, we find that the reaction free energies of this step on Fc-CPP-Cu and Bz-CPP-Cu are 0.89 and 0.92 eV, indicating that Fc-CPP-Cu has a slightly higher activity. As shown in Fig. 4a and b, the spin charge densities assigned to Cu in Fc-CPP-Cu and Bz-CPP-Cu are −0.58 e^- and −0.52 e^-, respectively. We find that after the introduction of the ferrocene group into the Fc-CPP-Cu structure, the reactivity of Cu in the porphyrin centre is enhanced relative to Bz-CPP-Cu, which agrees with the higher FE of Fc-CPP-Cu in the experimental results. Though the trend is right, we notice that the difference in the thermodynamic adsorption energies between Fc-CPP-Cu and Bz-CPP-Cu is still far tinier than the experimental differences. Therefore, a nudged elastic band (NEB) method was introduced to understand the efficiency differences impacted by Fc-CPP-Cu (Fig. 4d and e). We found that the activation energy of CO_2 protonation into *COOH for Fc-CPP-Cu (0.19 eV) was significantly lower than that of Bz-CPP-Cu (0.36 eV). We also

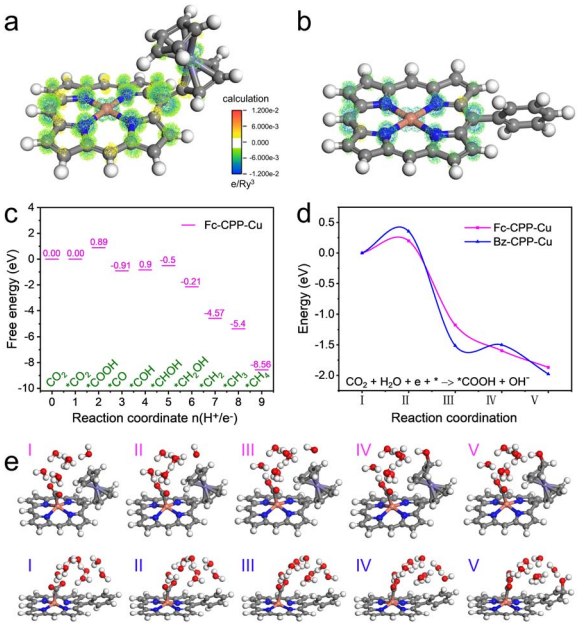

Fig. 4 (a) The DFT calculation and the proposed reaction mechanism. (a) The spin ($\rho_{up} - \rho_{down}$) of negative (green) and positive values (yellow) for Fc-CPP-Cu on Cu-porphyrin. (b) The spin ($\rho_{up} - \rho_{down}$) of negative (green) and positive values (yellow) for Bz-CPP-Cu on porphyrin-Cu. (c) Free energy profiles for the CO_2-to-CH_4 reaction pathway on Fc-CPP-Cu. It is plotted at a potential of −0.9 V *vs.* RHE. (d) The minimum energy path (MEP) calculated *via* a NEB calculation. (e) The reaction snapshots of different reaction coordinates in the CO_2RR for Fc-CPP-Cu and Bz-CPP-Cu.

conducted a simple calculation and found that this was due to the lower adsorption energy of the benzene ring for OH* than Fc-CPP-Cu, which means that Fc-CPP-Cu had better oxophilicity. This is based on Markovic's theory[46,47] that the strong adsorption capacity of ferrocene groups to OH* facilitates the PCET reaction process. Thus, the intrinsic advantage of Fc-CPP-Cu is due to the introduction of the ferrocene group as the oxophilic group that can kinetically improve the preference of the CO_2-to-CH_4 pathway. To support the DFT calculation results, *in situ* ATR-FTIR measurements have been conducted (Fig. 3c and d). The peaks at 1559 cm^{-1}, 1362 cm^{-1} and 1306 cm^{-1} can be ascribed to the asymmetric stretching, symmetric stretching, and stretching of C–O, respectively. In addition, the peak of chemisorbed CO (*CO) was detected at 2067 cm^{-1}, which is in good agreement with the most reported value (*i.e.* 2065 cm^{-1}) (Fig. 3c).[48,49] Furthermore, the signals appearing at 1041 cm^{-1} and 1456 cm^{-1} could be attributed to *COH and *CH_2O, respectively (Fig. 3d), which are key intermediates in the CO_2RR to CH_4 conversion.[48,49]

Conclusions

In summary, we have presented a scalable strategy to synthesize Cu-porphyrin based conjugated porous polymers and successfully applied them in efficient electrocatalytic CO_2RR. The obtained materials possessing high porosity (*e.g.*, Fc-CPP-Cu, S_{BET}, 144 $m^2\ g^{-1}$ and V_t, 0.18 $cm^3\ g^{-1}$), adjustable morphology (size, 250–500 nm) and high stability (strong covalent bond that enables long-term and stable electrocatalysis) are composed of directly bonded auxiliary groups and Cu-porphyrin centres. Specifically, Fc-CPP-Cu with ferrocene as the promoter group exhibits a $FE_{CH_4+C_2H_4}$ of 94.0% (FE_{CH_4}, 75.9% and FE_{C2H_4}, 18.1%, −0.9 V) and remains above 70% in a wide potential range from −0.7 to 1.0 V, which is much better than that of Cu-porphyrin, Bz-CPP-Cu and the physical mixture and represents one of the best CO_2 electroreduction catalysts so far. Moreover, the important role of the ferrocene group as the CO_2RR auxiliary and the detailed catalytic mechanism have been systematically investigated by DFT calculations. The results reveal that the directly interacting ferrocene groups could enhance the electron-cloud density of Cu in the porphyrin centre. Meanwhile, the strong adsorption ability of ferrocene groups to OH* promotes the PCET reaction process, which kinetically improves the preferential CO_2-to-CH_4 pathway. Noteworthily, the copolymerization strategy can be easily scaled up (∼10 g in a batch experiment) and the reaction time can be as little as 10 min under optimized microwave conditions. Generally, the exploration of high performance electrocatalysts that enable facile and scale-up production plays a vital role in the exploration of potential industrial scale electrocatalytic CO_2RR systems. This work has extended the potential scope of the microwave method in the production of metalloporphyrin based polymers that can be applied as efficient electrocatalytic CO_2-to-CH_4 electrocatalysts and explored the possible direct auxiliary bonding mechanisms. Despite the minor progress made in this work, it still has some unaddressed issues, for example, the industrial kilogram or ton scale production, the higher industrial demand current density or the generally neglected ultralow CO_2 conversion efficiency. All of these lie in the exploration of more advanced electrocatalytic CO_2RR techniques and powerful electrocatalysts that can address all of the potential issues related to industrial applications. As we can see, there is a long way to go from the laboratory work to real industrial applications. More efforts still need to be made for every vital setup of the electrocatalytic CO_2RR system and we believe it will be a powerful clean energy conversion system that might solve or mitigate energy and environmental crises to some extent.

Conflicts of interest

There are no conflicts to declare.

Acknowledgements

This work was financially supported by the NSFC (Grant No. 21871141, 21871142, 21901122, 22225109, 22071109, 22105080, 22171139, and 51978153).

Notes and references

1 D.-H. Yang, Y. Tao, X. Ding and B.-H. Han, *Chem. Soc. Rev.*, 2022, **51**, 761–791.
2 W. Ma, X. He, W. Wang, S. Xie, Q. Zhang and Y. Wang, *Chem. Soc. Rev.*, 2021, **50**, 12897–12914.
3 G. Wang, J. Chen, Y. Ding, P. Cai, L. Yi, Y. Li, C. Tu, Y. Hou, Z. Wen and L. Dai, *Chem. Soc. Rev.*, 2021, **50**, 4993–5061.
4 T. N. Nguyen and C.-T. Dinh, *Chem. Soc. Rev.*, 2020, **49**, 7488–7504.
5 R.-X. Yang, Y.-R. Wang, G.-K. Gao, L. Chen, Y. Chen, S.-L. Li and Y.-Q. Lan, *Small Struct.*, 2021, **2**, 2100012.
6 E. Fujita, D. C. Grills, G. F. Manbeck and D. E. Polyansky, *Acc. Chem. Res.*, 2022, **55**, 616–628.
7 Y.-R. Wang, H.-M. Ding, X.-Y. Ma, M. Liu, Y.-L. Yang, Y. Chen, S.-L. Li and Y.-Q. Lan, *Angew. Chem., Int. Ed.*, 2022, **61**, 202114648.
8 L. Fan, C.-Y. Liu, P. Zhu, C. Xia, X. Zhang, Z.-Y. Wu, Y. Lu, T. P. Senftle and H. Wang, *Joule*, 2022, **6**, 205–220.
9 S. R. Hui and P. De Luna, *Matter*, 2021, **4**, 1555–1577.
10 H. Gu, L. Zhong, G. Shi, J. Li, K. Yu, J. Li, S. Zhang, C. Zhu, S. Chen, C. Yang, Y. Kong, C. Chen, S. Li, J. Zhang and L. Zhang, *J. Am. Chem. Soc.*, 2021, **143**, 8679–8688.
11 N. G. Yasri, T. A. Al-Attas, J. Hu and M. G. Kibria, *Catal. Sci. Technol.*, 2021, **11**, 1580–1589.
12 Y.-R. Wang, M. Liu, G.-K. Gao, Y.-L. Yang, R.-X. Yang, H.-M. Ding, Y. Chen, S.-L. Li and Y.-Q. Lan, *Angew. Chem., Int. Ed.*, 2021, **60**, 21952–21958.
13 C. Hu, R. Paul, Q. Dai and L. Dai, *Chem. Soc. Rev.*, 2021, **50**, 11785–11843.
14 Y. Zhou, L. Zheng, D. Yang, H. Yang, Q. Lu, Q. Zhang, L. Gu and X. Wang, *Small Methods*, 2021, **5**, 2000991.
15 Q. Wu, M.-J. Mao, Q.-J. Wu, J. Liang, Y.-B. Huang and R. Cao, *Small*, 2021, **17**, 2004933.

16 A. Khaligh, Y. Sheidaei and D. Tuncel, *ACS Appl. Energy Mater.*, 2021, **4**, 3535–3543.
17 X.-D. Zhang, S.-Z. Hou, J.-X. Wu and Z.-Y. Gu, *Chem.–Eur. J.*, 2020, **26**, 1604–1611.
18 Q. Wu, R.-K. Xie, M.-J. Mao, G.-L. Chai, J.-D. Yi, S.-S. Zhao, Y.-B. Huang and R. Cao, *ACS Energy Lett.*, 2020, **5**, 1005–1012.
19 H. Xu, X. Chen, J. Gao, J. Lin, M. Addicoat, S. Irle and D. Jiang, *Chem. Commun.*, 2014, **50**, 1292–1294.
20 Y. Lu, J. Zhang, W. Wei, D.-D. Ma, X.-T. Wu and Q.-L. Zhu, *ACS Appl. Mater. Interfaces*, 2020, **12**, 37986–37992.
21 E. M. Johnson, R. Haiges and S. C. Marinescu, *ACS Appl. Mater. Interfaces*, 2018, **10**, 37919–37927.
22 X. Yuan, Q. Mu, S. Xue, Y. Su, Y. Zhu, H. Sun, Z. Deng and Y. Peng, *J. Energy Chem.*, 2021, **60**, 202–208.
23 Z. Xin, Y.-R. Wang, Y. Chen, W.-L. Li, L.-Z. Dong and Y.-Q. Lan, *Nano Energy*, 2020, **67**, 104233.
24 A. Sengupta, S. Datta, C. Su, T. S. Herng, J. Ding, J. J. Vittal and K. P. Loh, *ACS Appl. Mater. Interfaces*, 2016, **8**, 16154–16159.
25 J. Behler, *Angew. Chem., Int. Ed.*, 2017, **56**, 12828–12840.
26 J. Behler and M. Parrinello, *Phys. Rev. Lett.*, 2007, **98**, 146401.
27 K. Walter, *Phys. Rev. Lett.*, 1996, **76**, 3168–3171.
28 H.-F. Wang, L. Chen, H. Pang, S. Kaskel and Q. Xu, *Chem. Soc. Rev.*, 2020, **49**, 1414–1448.
29 G. Singh, J. Lee, A. Karakoti, R. Bahadur, J. Yi, D. Zhao, K. AlBahily and A. Vinu, *Chem. Soc. Rev.*, 2020, **49**, 4360–4404.
30 H. Feng, X. Liu, Y. Li, X. Ma, Q. Yan and F. Zhao, *Powder Technol.*, 2022, **397**, 117035.
31 H. Li, N. Meng, W. Lyu, Z. Cheng, S. Chen, W. Zhang and Y. Liao, *J. Colloid Interface Sci.*, 2021, **595**, 178–186.
32 Z. Xu, Q. Mei, Q. Hua, R. Tian, J. Weng, Y. Shi and W. Huang, *J. Mol. Struct.*, 2015, **1094**, 1–8.
33 S. Yuan, L.-L. Cui, Z. Dou, X. Ge, X. He, W. Zhang and T. Asefa, *Small*, 2020, **16**, 2000742.
34 G. Mei, L. Cui, Z. Dou and X. He, *Electrochim. Acta*, 2020, **358**, 136918.
35 L.-L. Zhou, Q. Guan, W.-Y. Li, Z. Zhang, Y.-A. Li and Y.-B. Dong, *Small*, 2021, **17**, 2101368.
36 W. Zhang, T. Cui, L. Yang, C. Zhang, M. Cai, S. Sun, Y. Yao, X. Zhuang and F. Zhang, *J. Colloid Interface Sci.*, 2017, **497**, 108–116.
37 Q. Lin, X. Bu, A. Kong, C. Mao, F. Bu and P. Feng, *Adv. Mater.*, 2015, **27**, 3431–3436.
38 X.-F. Qiu, H.-L. Zhu, J.-R. Huang, P.-Q. Liao and X.-M. Chen, *J. Am. Chem. Soc.*, 2021, **143**, 7242–7246.
39 J. Liu, D. Yang, Y. Zhou, G. Zhang, G. Xing, Y. Liu, Y. Ma, O. Terasaki, S. Yang and L. Chen, *Angew. Chem., Int. Ed.*, 2021, **60**, 14473–14479.
40 H. Zhong, M. Ghorbani-Asl, K. H. Ly, J. Zhang, J. Ge, M. Wang, Z. Liao, D. Makarov, E. Zschech, E. Brunner, I. M. Weidinger, J. Zhang, A. V. Krasheninnikov, S. Kaskel, R. Dong and X. Feng, *Nat. Commun.*, 2020, **11**, 1409.
41 C. Wang, H. Tissot, M. Soldemo, J. Lu and J. Weissenrieder, *J. Nano Res.*, 2022, **15**, 709–715.
42 D. M. Weekes, D. A. Salvatore, A. Reyes, A. Huang and C. P. Berlinguette, *Acc. Chem. Res.*, 2018, **51**, 910–918.
43 X. She, T. Zhang, Z. Li, H. Li, H. Xu and J. Wu, *Cell Rep. Phys. Sci.*, 2020, **1**, 100051.
44 C. M. Gabardo, C. P. O'Brien, J. P. Edwards, C. McCallum, Y. Xu, C.-T. Dinh, J. Li, E. H. Sargent and D. Sinton, *Joule*, 2019, **3**, 2777–2791.
45 S. Chen, Y. Su, P. Deng, R. Qi, J. Zhu, J. Chen, Z. Wang, L. Zhou, X. Guo and B.-Y. Xia, *ACS Catal.*, 2020, **10**, 4640–4646.
46 D. Strmcnik, M. Uchimura, C. Wang, R. Subbaraman, N. Danilovic, D. van der Vliet, A. P. Paulikas, V. Stamenkovic and N. M. Markovic, *Nat. Chem.*, 2013, **5**, 300–306.
47 D. Strmcnik, P. P. Lopes, B. Genorio, V. R. Stamenkovic and N. M. Markovic, *Nano Energy*, 2016, **29**, 29–36.
48 S. Zhu, T. Li, W.-B. Cai and M. Shao, *ACS Energy Lett.*, 2019, **4**, 682–689.
49 J.-D. Yi, R. Xie, Z.-L. Xie, G.-L. Chai, T.-F. Liu, R.-P. Chen, Y.-B. Huang and R. Cao, *Angew. Chem., Int. Ed.*, 2020, **59**, 23641–23648.

